AGU ADVANCING EARTH AND SPACE SCIENCE

Geophysical Research Letters

RESEARCH LETTER
10.1029/2021GL093151

Key Points:

- Quantitative determination of prompt and global outer-belt responses for two MeV electron injection events
- Large step-like outer-belt relativistic electron enhancements on ~30-min time scales nearly instantaneously with the injections
- The extremely fast step-like outer-belt enhancements for the two events are most-likely injection-driven

Supporting Information:

Supporting Information may be found in the online version of this article.

Correspondence to:

H.-J. Kim,
heekim@atmos.ucla.edu

Citation:

Kim, H.-J., Lee, D.-Y., Wolf, R., Bortnik, J., Kim, K.-C., Lyons, L., et al. (2021). Rapid injections of MeV electrons and extremely fast step-like outer radiation belt enhancements. *Geophysical Research Letters*, *48*, e2021GL093151. https://doi.org/10.1029/2021GL093151

Received 5 MAR 2021
Accepted 27 APR 2021

Rapid Injections of MeV Electrons and Extremely Fast Step-Like Outer Radiation Belt Enhancements

H.-J. Kim[1], D.-Y. Lee[2], R. Wolf[3], J. Bortnik[1], K.-C. Kim[2], L. Lyons[1], W. Choe[4], S.-J. Noh[5], K.-E. Choi[2], C. Yue[6], and J. Li[1]

[1]Department of Atmospheric and Oceanic Sciences, University of California, Los Angeles, CA, USA, [2]Department of Astronomy and Space Science, Chungbuk National University, Cheongju, South Korea, [3]Department of Physics and Astronomy, Rice University, Houston, TX, USA, [4]May & June Solutions, Jung-Gu, Seoul, South Korea, [5]Center for Solar-Terrestrial Research, New Jersey Institute of Technology, Newark, NJ, USA, [6]School of Earth and Space Science, Peking University, Beijing, China

Abstract Rapid injection of MeV electrons associated with strong substorm dipolarization has been suggested as a potential explanation for some radiation belt enhancement events. However, it has been difficult to quantify the contribution of MeV electron injections to radiation belt enhancements. This paper presents two isolated MeV electron injection events for which we quite precisely quantify how the entire outer-belt immediately changed with the injections. Tracking detailed outer-belt evolution observed by Van Allen Probes, for both events, we identify large step-like relativistic electron enhancements (roughly 1 order of magnitude increase for ~2 MeV electron fluxes) for $L \gtrsim 3.8$ and $L \gtrsim 4.6$, respectively, that occurred on ~30-min time scales nearly instantaneously with the injections. The enhancements occurred almost simultaneously for 10s keV to multi-MeV electrons, with the lowest L of enhancement region located farther out for higher energy. The outer-belt stayed at these new levels for ≳several hours without substantial subsequent enhancements.

Plain Language Summary Since the discovery of the Earth's radiation belts, the populations of energetic particles trapped by the magnetic fields, understanding the origin of radiation belt relativistic electrons has been one of the primary goals in space physics. One proposal for their source is that relativistic electrons are rapidly injected from outside the radiation belts associated with dramatic changes of the background magnetic field. To explore the importance of this process, we conduct a case study of two isolated injection events. With a new analysis technique, we quite precisely determine how the entire radiation belt electron population immediately changed with the injections. For both events, we find large, step-like relativistic electron enhancements in a significant part of the outer radiation belt. The enhancements occurred promptly with the injections on extremely fast time scales that are comparable to the injection process. Furthermore, they occurred almost simultaneously for a wide energy range, showing an energy-dependent feature that can be explained by injection process. After the enhancements, the outer-belt relativistic electron intensities stayed at the enhanced levels for at least several hours without substantial subsequent enhancements, indicating that the enhancements occurred discretely with the injections.

1. Introduction

The origin of radiation belt relativistic electrons has been an intriguing scientific question since their discovery in 1958 (Van Allen et al., 1958, 1959). Two currently prevailing views for their origin are adiabatic acceleration of plasma sheet electrons during diffusive inward radial transport by fluctuating electric and magnetic fields (e.g., Brautigam & Albert, 2000; Kellogg, 1959; Millan & Baker, 2012, and references therein) and local acceleration of electrons in the radiation belts via repeated gyro-resonant interactions with whistler-mode chorus waves (e.g., Horne et al., 2005; Summers et al., 1998; Thorne et al., 2013).

One compelling alternative view is rapid injection of MeV electrons from the tail associated with strong substorm-induced electric fields (e.g., Dai et al., 2014; Fok et al., 2001; Ingraham et al., 2001; Kim et al., 2000; Nagai et al., 2006; Sorathia et al., 2018). Although this process has received less attention as a crucial contributor to radiation belt enhancements, several simulations have demonstrated its capability of supplying

relativistic electrons to the trapped region of the inner magnetosphere on extremely fast time scales (~few 10 min) (e.g., Fok et al., 2001; Glocer et al., 2011; Kress et al., 2014; Sorathia et al., 2018). Furthermore, some observational analyses have suggested that injections may account for not only rapid rebuilding of the core part of the outer-belt during the storm main phase (e.g., Nagai, 2012), but also a delayed buildup at geosynchronous altitudes during storm recovery with prolonged substorm activity (e.g., Ingraham et al., 2001).

Recently, utilizing high-quality radiation belt observations by the Van Allen Probes (Mauk et al., 2013), several studies revisited the significance of MeV electron injections. Dai et al. (2015) and Tang et al. (2016) examined rapid (~1–3-h time scales) outer-belt enhancement events that occurred with clear signatures of substorm injection of MeV electrons. Without strong activity of local whistler waves and global ULF waves during the events, they concluded that MeV electron injections are likely primarily responsible for the enhancements. However, for a similar type of event, Liu et al. (2018) suggested a different scenario that electrons are first locally accelerated in the near-Earth plasma sheet via wave-particle interactions, and then further accelerated by rapid radial diffusion into the outer-belt. On the other hand, Foster et al. (2014) and Su et al. (2014) examined events with strong chorus wave activity which were also accompanied by MeV electron injections, and concluded that the rapid flux enhancements on several hour time scales were mostly attributable to local wave acceleration. However, Su et al. (2014) noted that the contribution of injections is difficult to assess when multiple injections (which are common (e.g., Borovsky & Yakymenko, 2017)) are involved. These conflicting explanations and limitations in the analysis illustrate the difficulty of unambiguously evaluating the relative contribution of MeV electron injections and determining a dominant process for given radiation belt enhancements.

Given that injections would tend to occur over extremely fast time scales, appearing discretely at times of strong dipolarization, if we could examine rapid responses of the entire radiation belt for well-isolated injection events, it may provide new insights into the significance of the injection process. With that goal, this study focuses on two distinctly isolated MeV electron injection events to which prompt, global radiation belt changes were unprecedentedly well-observed by the Van Allen Probes. With a new analysis technique to closely track detailed outer-belt evolution, for both events, we quite precisely determine how much, how fast, over which L-region, and up to which electron energy outer-belt enhancements took place and how they are related to the injections.

2. MeV Electron Injections and Extremely Fast Radiation Belt Electron Enhancements

In NASA's recent Van Allen Probes mission, two identical satellites monitored the full L-shell range of the radiation belts on average every ~4.5 h, following each other on nearly identical, near-equatorial, highly elliptical orbits with a time delay that varied from ~10s min to a half orbit (Mauk et al., 2013). Owing to this unique orbital configuration, for some electron enhancement or loss events that the two satellites happened to observe at the right locations and at the right times, based only on the data from these two satellites, we can reconstruct how the entire radiation belt might have evolved, even on substorm time scales of ~10s min. Here, we examine two such well-observed radiation belt enhancement events, primarily analyzing spin-averaged electron fluxes from the Magnetic Electron Ion Spectrometer (MagEIS; Blake et al., 2013) and Relativistic electron Proton Telescope (REPT; Baker et al., 2012) of the Energetic Particle Composition and Therma Plasma (ECT) suite (Spence et al., 2013) on board the Van Allen Probes.

2.1. Event 1 on September 27, 2016

In Figure 1a, the first event (Event 1) occurred on September 27, 2016, associated with extremely strong substorm activity (SuperMAG electrojet (SME) index peak ~ 2,171 nT) during a fairly weak geomagnetic storm (Dst ~ −40 nT). Here, SME is an equivalent to the AE index, constructed from >100 magnetometer stations (Newell & Gjerloev, 2011). Figure 1b shows the electron fluxes observed by Van Allen Probes B (P-B) near apogee at ~1.3 MLT (see Figure S1 in the Supporting Information for satellites' locations). With the exceptionally large SME increase, P-B observed sudden large flux increases at ~14:57 UT for all the energies up to 3.4 MeV (dotted line). Energy-dispersed drift echoes are discernable for 210 –743 keV fluxes. Such energy dispersion is a well-known injection signature resulting from the energy-dependent magnetic

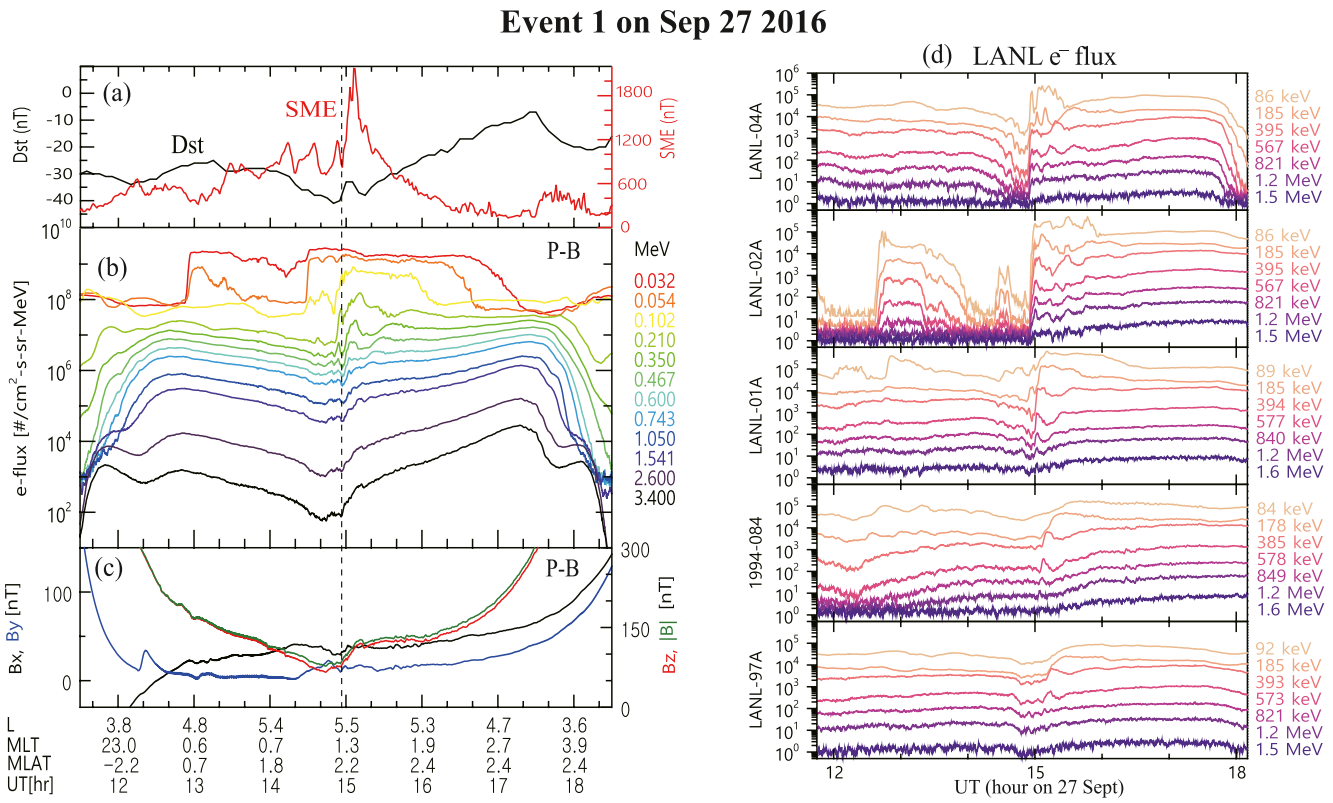

Figure 1. Injection event, Event 1, on September 27, 2016. (a) Dst index (black) and SME (red). (b and c) Spin-averaged electron flux from MagEIS (≤1.541 MeV) and REPT (≥2.1 MeV) and magnetic field from the Electric and Magnetic Field Instrument Suit and Integrated Science (EMFISIS) fluxgate magnetometer (Kletzing et al., 2013) on board P-B, respectively. The dotted line denotes the sudden flux increase at ~14:57 UT. (d) Electron flux (#/cm^2 s sr keV) from five Los Alamos National Laboratory geosynchronous (LANL-GEO) satellites. SME, SuperMAG electrojet; MagEIS, Magnetic Electron Ion Spectrometer; REPT, Relativistic electron Proton Telescope.

drift (e.g., Reeves et al., 1991). Similar energy dispersion is hard to identify for MeV fluxes most likely due to the faster drift speed of MeV electrons (drift period ≲10 min). Figure 1c shows that these flux increases are accompanied by large increases in $|B|$ and B_z, implying magnetic field dipolarization. Van Allen Probes A (P-A) did not observe the flux enhancement, since it was located at lower L-shells, near the slot region.

The injection signatures of Event 1 were more clearly observed by LANL geosynchronous satellites (see Figure S1a for their locations). In Figure 1d, LANL-04A, which was located at ~19.4 MLT at ~14:55 UT, observed sharp dispersionless flux increases at all the energies up to 1.5 MeV (i.e., injection front). Immediately following this, LANL-02A at ~24 MLT observed only very slightly dispersed flux increases. Then, more pronounced energy dispersion with longer delays (though weaker at higher energies) were observed by the other eastward satellites, LANL-01A, 1994-084, and LANL-97A at ~04, ~12, and ~15.5 MLT, respectively. Earlier in Figure 1b, P-B at ~1.3 MLT observed sudden flux increases at ~14:57 UT, which is ~2 min after LANL-04A at ~19.4 MLT observed the injection front. Considering the relative location of P-B to the LANL satellites in Figure S1a, ~2-min delay is consistent with the successively delayed, dispersed flux increases shown in Figure 1d. The dispersed flux increases were also clearly observed by GOES satellites, as shown in Figure S2 in the Supporting Information. All these observations confirm that the flux increases of Event 1 are indeed a substorm injection.

Now an important question is how much flux increased at other L-shells when P-B near apogee observed the large flux increase in Figure 1b. This basically asks about how the entire radiation belt electron intensities immediately changed with the injection. Fortunately for Event 1, we can derive such information from Van Allen Probes observations. To intuitively visualize any extremely fast outer-belt changes that occurred globally, we employ a so-called hourly snapshot technique where we simultaneously track electron flux

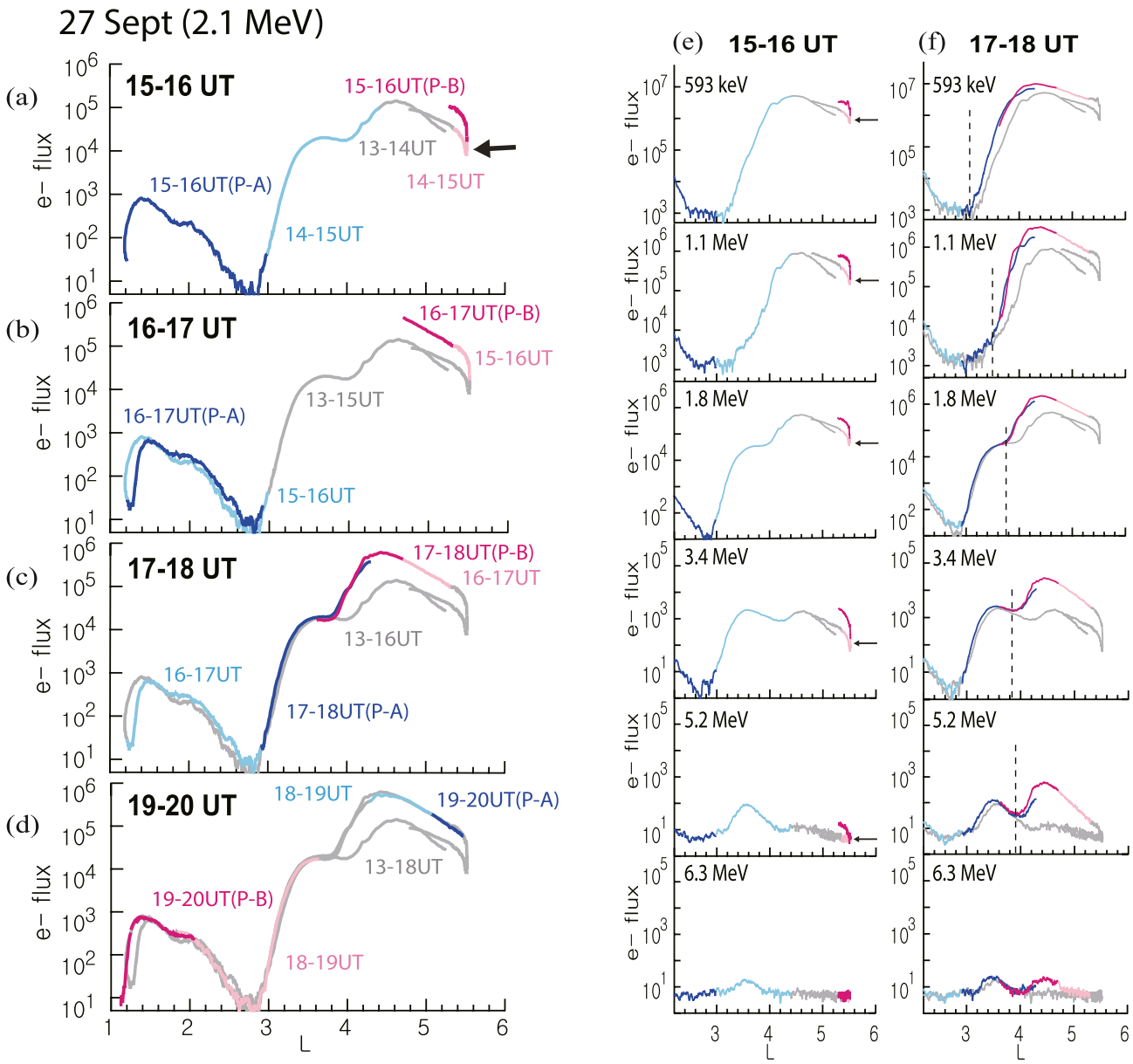

Figure 2. Hourly snapshots of electron flux vs. *L* for Event 1. (a–d) Hourly flux snapshots for 2.1 MeV for 15–16 UT, 16–17 UT, 17–18 UT, 19–20 UT, respectively: Blue and pink denote the electron flux traces for the current 1 h and light blue and light pink for the previous 1 h, observed by P-A (bluish) and P-B (pinkish), while gray the earlier hour(s) for both satellites. (e–f) Hourly snapshots for 15–16 UT and 17–18 UT, respectively, for 539 keV to 6.3 MeV. Black arrows denote the sudden flux increase, and dotted lines the lowest *L*-shell of enhancement. Hourly flux snapshots use spin-averaged electron flux (#/cm^2 s sr MeV) from MagEIS (≤1.1 MeV) or/and REPT (≥1.8 MeV). MagEIS, Magnetic Electron Ion Spectrometer; REPT, Relativistic electron Proton Telescope.

changes observed by both satellites, plotting them in the same parameter space of flux vs. *L* over a short-time interval of 1 h that is sequentially advanced by 1-h time step, while keeping previous traces on the plot.

In Figure 2, the radiation belt evolution for Event 1 is examined with the hourly snapshot technique. Figures 2a–2d show the hourly snapshots of flux vs. *L* plot for 2.1 MeV, where fluxes are traced from 13 UT, ~2 h before Event 1. In each snapshot, blue and pink denote the electron flux traces for the current 1 h and light blue and light pink for the previous 1 h, observed by P-A (bluish) and P-B (pinkish), while gray denotes the earlier hour(s) for both satellites. From the hourly sequences of the flux evolution in Figures 2a–2d, we can identify the followings:

1. 15–16 UT snapshot: When outbound P-B (light pink) almost reached apogee, it started to observe a sudden flux increase (arrow) which corresponds to the flux increase at ∼14:57 UT in Figure 1b (dotted line). P-B (pink) at apogee continues to observe increasing flux, and then becomes an inbound pass at ∼15:25 UT. Note that during this hour P-A (blue) was mostly in the inner-belt
2. 16–17 UT snapshot: Inbound P-B (pink) traverses the outer part of the outer-belt, observing several times larger electron fluxes than those (gray curve below pink) observed earlier during 13–14 UT. We cannot determine whether or not the electron flux is still increasing solely from this inbound P-B′s trace, because we cannot distinguish between (if any) a pure temporal flux increase and a mere spatial effect from the nominal outer-belt radial profile that electron fluxes increase toward the center of the outer-belt, i.e., negative radial gradient
3. 17–18 UT snapshot: However, by tracking further in time, we can deduce the end time of the flux increase. P-A (blue) finally comes out to the outer-belt and observes about the same flux levels that P-B observes/observed at different times (i.e., overlap of pink and blue)
4. 19–20 UT snapshot: P-A continues to observe roughly the same flux levels that P-B observed earlier all the way to apogee, i.e., overlap of the bluish and top gray curves. The overlap indicates that no significant flux changes occurred after P-B left apogee at ∼15:25 UT. In other words, the large flux increase, which started at ∼14:57 UT in Figure 2a, was completed at ∼15:25 UT. As seen in Figure 2c, over that extremely brief time of ∼28 min, a large part of the outer-belt got significantly enhanced. Specifically, the 2.1 MeV flux for $L \gtrsim 3.8$ increased by ∼1 order of magnitude, with the maximum increase (in ratio) at $L \sim 4.2$. The enhancement moved the flux peak a bit earthward from $L \sim 4.6$ (the preenhancement radial profile in gray) to $L \sim 4.4$

Here, it is interesting to note that the enhancement occurred discretely with the injection. As indicated by the top overlapped traces for $L \gtrsim 3.8$ in Figures 2c and 2d, no substantial subsequent flux increases occurred during ∼15:25 UT to ∼20 UT after Event 1, leaving the electron flux at the enhanced level (by Event 1) for at least ∼4.5 h. The sharply turned-on and turned-off, discrete, step-like outer-belt enhancement of Event 1 would be difficult to be explained by the usual local wave acceleration or radial diffusion processes which would typically require a few hours to achieve substantial acceleration (Agapitov et al., 2019), but could be accounted for by impulsive dipolarization-driven radial transport.

The association of Event 1 with substorm injection is also clear, when other energy channels are examined. Figures 2e and 2f show the hourly flux snapshots for 15–16 UT and 17–18 UT, respectively, for various energies from 593 keV to 6.3 MeV. As indicated by the arrows in the 15–16 UT snapshots, similar to Figure 2a, sudden flux increase is observed almost simultaneously for all the energies except for 6.3 MeV. Then, the 17–18 UT snapshots show the significantly enhanced outer-belt for each energy up to 5.2 MeV, while only slightly enhanced for 6.3 MeV (note the different y axis scales). The dotted lines denote the lowest L-shell up to which the enhancement occurred for each energy. Remarkably, the lowest L-shell is located farther out for higher energy, which is consistent with the well-known energy-dependent substorm injection boundary (e.g., Pfitzer & Winkler, 1968; Reeves et al., 2016). This energy-dependent inner boundary feature further indicates that the outer-belt enhancement of Event 1 is likely to be injection-driven.

2.2. Event 2 on September 19, 2013

As shown in Figure 3a, the second event (Event 2) occurred on September 19, 2013 also in association with a strong substorm activity (SME peak ∼ 1,450 nT), though weaker than that for Event 1, and under practically a nonstorm time condition (Dst > −25 nT). For Event 2, while P-A was located in the inner-belt, P-B was located near apogee in the early evening sector of ∼18 MLT. Figure 3b indicates that P-B observed flux increases starting at ∼08:37 UT (dotted line) for most of the energies up to 2.6 MeV. Distinct echo signatures of injections are discernible only for 132 and 210 keV. Despite that, the occurrence of substorm-associated MeV electron injection is supported by GOES observation of geosynchronous injection around the SME peak. As shown in Figure S3 in the Supporting Information, GOES-13 at ∼04 MLT observed dispersed flux increase at ∼08:30 UT, which is ∼7 min earlier than that seen by P-B at $L \sim 5.2$ and ∼18 MLT. With the relative location of GOES-13 to P-B and the earthward propagation and azimuthal drift speed taken into account, ∼7-min delay seems reasonable.

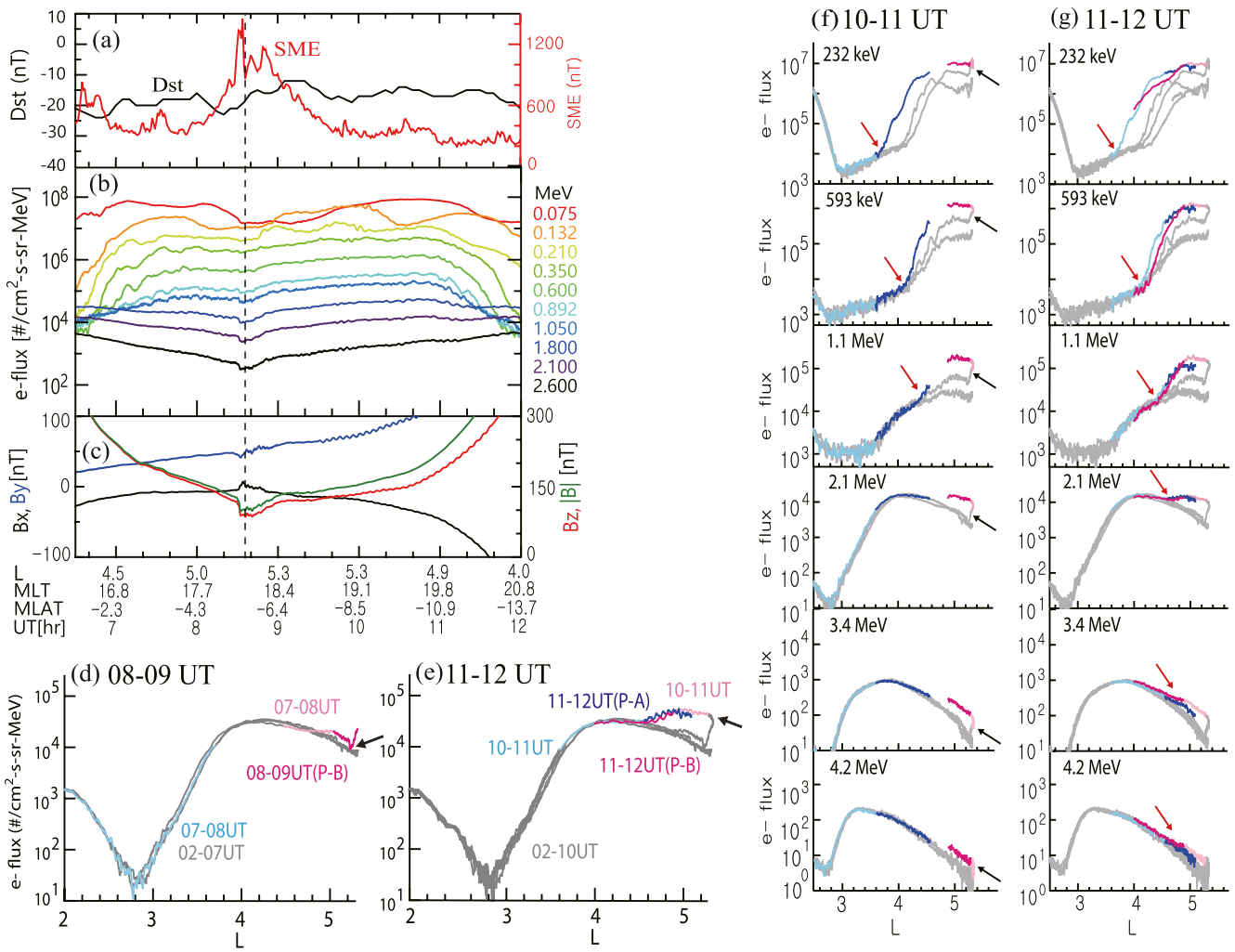

Figure 3. Injection event, Event 2, on September 19, 2013. (a–c) Similar to Figure 1, Dst (black) and SME (red), spin-averaged electron flux from MagEIS and REPT, and magnetic field from EMFISIS onboard P-B, respectively. The dotted line denotes the flux increase at 08:37 UT. (d–e) 08–09 UT and 11–12 UT hourly flux snapshots for 1.8 MeV, respectively. (f–g) 10–11 UT and 11–12 UT hourly snapshots for 232 keV to 4.2 MeV, respectively. For each energy (<4.3 MeV), black arrows denote the sudden flux increase, and red arrows the lowest L-shell of enhancement. SME, SuperMAG electrojet; MagEIS, Magnetic Electron Ion Spectrometer; REPT, Relativistic electron Proton Telescope.

To demonstrate the nature of the flux increase of Event 2 more effectively, Figures 3d and 3e show the 08–09 UT and 11–12 UT flux snapshots for 1.8 MeV, respectively. In the 08–09 UT snapshot, outbound P-B (pink) starts to observe a sudden flux increase at ~08:37 UT (arrow) which corresponds to the dotted line in Figure 3b. Similar to Event 1, we can determine the completion time of the flux increase by tracking further in time. In the 11–12 UT snapshot in Figure 3e, the bluish (outbound P-A) and the pinkish (inbound P-B) curves roughly overlap with each other, indicating that the two satellites observed similar flux levels at the same L-shells at different times. As noted earlier, such overlap indicates no occurrence of significant flux changes during the satellites' traversals. The overlap roughly continues until P-A reaches apogee (not shown), from which we can reasonably verify that the flux increase completed at ~09:10 UT which is the time when P-B left apogee (arrow in Figure 3e). Accordingly, Event 2 only took place over a span of ~33 min from ~08:37 UT to 09:10 UT. As illustrated in Figure 3e, the 1.8 MeV electron flux for $L \gtrsim 4.6$ got enhanced by up to ~1 order of magnitude, moving the flux peak to $L \sim 5$ from its previous location at $L \sim 4.2$.

Similar to Event 1, examination of other energy channels further helps to understand the association with substorm injection. Figures 3f and 3g present the hourly flux snapshots for 10–11 UT and 11–12 UT,

respectively, for energies from 232 keV to 4.2 MeV. In the 10–11 UT snapshots, as indicated by black arrows, sudden large flux increase is observed almost simultaneously at all energies except for 4.2 MeV for which only slight increase is observed. In the same snapshot, during 10–11 UT, while inbound P-B (pink) observes enhanced electron fluxes at larger L-shells (i.e., pink above gray) for all the energies, outbound P-A (blue), which just moved out to the outer-belt, observes enhanced fluxes only for the energies of $\lesssim$~1.1 MeV (red arrows). In the next hour, in the 11–12 UT snapshots, when P-A moved farther out, it now observes enhanced fluxes even at higher energies (>1.1 MeV). As indicated by the red arrows, outbound P-A started to observe increased fluxes successively later with increasing energy. Earlier in Figure 3e, we deduced that the flux increase was completed at ~09:10 UT, which means that in the 10–11 UT snapshots in Figure 3f, the outbound P-A merely observes already increased fluxes. In other words, the outbound P-A's delayed observations of flux increases for higher energies (red arrows) are not a temporal but a spatial feature resulting from the fact that the lowest L-shell where flux increase occurred is located farther out for higher energy. Similar to Event 1, this is consistent with the energy-dependent substorm injection boundary effect, supporting the hypothesis that the outer-belt enhancement of Event 2 is also likely primarily injection-driven. Importantly, without the inbound P-B's observation in Figure 3f (pinkish traces), P-A's delayed observation of higher-energy electron flux increase could have been misinterpreted as delayed acceleration of higher-energy electrons, as proposed in the local wave acceleration scenario where 10s–100s keV plasma sheet electrons are first injected and then accelerated to relativistic energies through wave-particle interactions with a time delay of several hours (e.g., Baker et al., 1998; Summers et al., 1998; Thorne et al., 2013).

Event 2 is particularly interesting in that it shows that significantly large relativistic electron enhancement occurred even under nearly nonstorm condition. Such nonstorm time outer-belt enhancements, which mostly occurred during high-speed solar wind streams, have been reported in earlier studies (e.g., Anderson et al., 2015; Kim et al., 2015; Pinto et al., 2018; Schiller et al., 2014). However, the overall extent of enhancement for Event 1 that occurred associated with much stronger substorm under relatively stronger storm condition is considerably larger than that for Event 2. Specifically, the radial extent of enhancement is much larger for Event 1 than for Event 2. For example, the enhancement region for 593 keV electron flux is $L \gtrsim 3$ for Event 1 (Figure 2f) vs. $L \gtrsim 4.2$ for Event 2 (Figure 3g), while that for 2.1 MeV electron flux is $L \gtrsim 3.8$ for Event 1 (Figure 2c) vs. $L \gtrsim 4.6$ for Event 2 (Figure 3g). This can be attributable to the fact that the substorm-induced electric field strength, which can control how deep electrons get injected into the radiation belts, would be much larger for Event 1 (Reeves et al., 2016). Likewise, the radial position of the maximum electron flux (L_{jmax}) is located at lower L for Event 1. Tverskaya (1996) noted the modulation of L_{jmax} with $|\mathrm{Dst}_{\mathrm{min}}|$ on inverse power-law functional relationship. Furthermore, the highest energy for enhancement is larger for Event 1 (~5.2 MeV) than for Event 2 (~3.4 MeV), and the maximum flux increase for 2.1 MeV is larger for Event 1 (a factor of ~11 at $L \sim 4.2$) than for Event 2 (a factor of ~8 at $L \sim 5.3$). These enhancement properties can be also affected by the level of preexisting electron intensity.

We stress here that, for both events, if the Van Allen Probes satellites had not been at the right locations at the times of injection, we would not have been able to identify the sudden occurrences of step-like outer-belt enhancement, nor thereby precisely determine their timings and time scales, nor the energy-dependent inner boundary feature, which are all critical information for understanding their association with injection.

2.3. Phase Space Density Radial Profile and Significance of MeV Electron Injection

Owing to its occurrence under prolonged, relatively quiet geomagnetic condition, Event 2 provides a good opportunity to reliably estimate phase space density (PSD) radial profiles for outer-belt relativistic electrons, without largely affected by magnetic field model errors. To determine whether the PSD radial profile for Event 2 is consistent with inward radial transport, we examine PSD evolution using the hourly snapshot technique. Figures 4a (the same as Figure 3e) and 4b show the 11–12 UT flux snapshot for 1.8 MeV and its corresponding (in terms of time) PSD snapshot for $\mu = 2{,}000$ MeV/G and $K = 0.05\ \mathrm{G}^{1/2}R_{\mathrm{E}}$, respectively. As denoted by arrows in the figures, there is a distinct PSD increase corresponding to the large flux increase of Event 2. The PSD enhancement indicates that the flux increase is not merely an adiabatic effect. As described earlier, the top overlapped flux traces in Figure 4a indicate no occurrence of significant flux changes during the respective satellite traversals. Correspondingly, the overlapped pinkish and bluish PSD traces in Figure 4b indicate that the inbound P-B (pinkish) and the outbound P-A (bluish) observed roughly the same

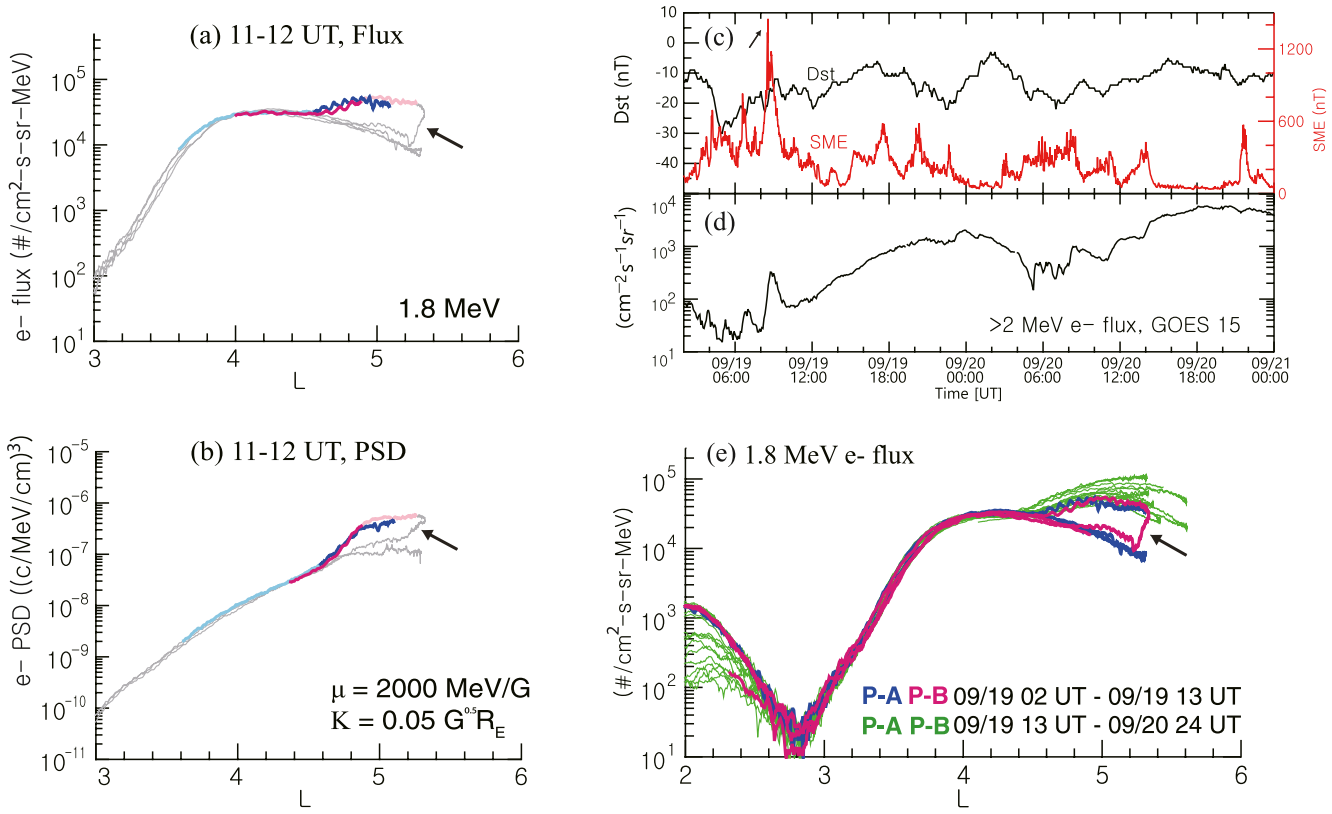

Figure 4. (a and b) 11–12 UT flux snapshot for 1.8 MeV and 11–12 UT PSD snapshot for μ = 2,000 MeV/G and $K = 0.05G^{1/2}R_E$ for Event 2, respectively. Black arrows denote the sudden flux increase of Event 2 and its corresponding PSD increase, respectively. (c) Dst (black) and SME (red). Arrow indicates the SME peak associate with Event 2. (d) Integral electron flux for >2 MeV from GOES 15. (e) Electron flux traces for 1.8 MeV, where blue (P-A) and pink (P-B) denote the traces for 02–13 UT on September 19 until right after Event 2 and the green (both P-A and P-B) for 13 UT on September 19 to 24 UT on September 20. SME, SuperMAG electrojet.

PSDs at same L's at different times, i.e., no temporal variations. Therefore, the overlapped PSD traces can reasonably represent the purely spatial structure of the post-enhancement PSD. Clearly, Figure 4b indicates the outwardly increasing PSD, which is consistent with inward radial transport. The PSDs in Figure 4b were computed using OP77Q magnetic field model (Olson & Pfitzer, 1977), and we can obtain similar PSD profiles for different models such as T89D and T89Q (Tsyganenko, 1989), and TS04D (Tsyganenko & Sitnov, 2005). However, it is not the case for Event 1, which makes it difficult to reliably determine the PSD radial profile for Event 1.

Event 2 also provides a rare opportunity to quickly gauge the significance of MeV electron injection for the overall radiation belt enhancement. The Dst and SME time series in Figure 4c illustrate the long-term geomagnetic condition around Event 2, where the outstandingly large SME increase associated with Event 2 (arrow) is followed by mostly mild and moderate substorms during a prolonged, nearly nonstorm time interval. Under this condition, we can reasonably evaluate how much the electron enhancement of Event 2 accounts for the total outer-belt enhancement that occurred over the ~2-days time interval shown in Figure 4c. Figure 4d indicates that the >2 MeV electron flux observed by GOES 15 increased by almost 2 orders of magnitude during the ~2-day period. For the same time interval, Figure 4e shows the 1.8 MeV electron flux traces observed by Van Allen Probes, where blue (P-A) and pink (P-B) denote the traces for approximately half a day until right after Event 2 and green (both P-A and P-B) denotes the rest of the time interval after Event 2. Remarkably, in Figure 4e, the flux increase of Event 2 (arrow), which only occurred over a span of ~33 min, roughly accounts for more than a half of the total flux increase (in log value) that took place over the entire period of ~2 days. Although it might be limited to nearly nonstorm time cases, this observation suggests that strong dipolarization-associated MeV electron injections, if occur in a series, could be an important source of outer-belt enhancements. In Figure 4e, during the rest of the time after

Event 2 (green traces), the flux gradually built up on top of the enhancement of Event 2, for which simultaneous operation of radial diffusion and local wave acceleration processes may be expected.

A similar examination of long-term (2-days) outer-belt evolution for Event 1 is described in Text S1 along with Figure S4 in the supporting information. Unlike for Event 2, the outer-belt underwent large flux increases and decreases after Event 1, associated with the persistent geomagnetic activities. However, as indicated in Figure S4d, some portion of the electron enhancement of Event 1 was still sustained, accounting for quite a significant amount of the total outer-belt enhancement that occurred over the 2-days time interval.

3. Conclusion

We examined two MeV electron injection events associated with extremely strong substorm activity under fairly small storm disturbance and very strong but relatively weaker substorm under nearly nonstorm condition, respectively. With the so-called hourly snapshot technique, we quite precisely determined how the entire outer-belt rapidly changed with the injections. For both events, we discovered the following essential features:

1. Nearly instantaneously with the injections, large step-like relativistic electron enhancements occurred in a significant part of the outer-belt, e.g., roughly 1 order of magnitude increase for ~2 MeV electron flux for $L \gtrsim 3.8$ and $L \gtrsim 4.6$, respectively
2. The enhancements occurred over ~30-min time scales, discretely with the injections. That is, the outer-belt promptly enhanced with the injections and then stayed at the enhanced level for $\gtrsim$ several hours, without substantial subsequent enhancements
3. The enhancements occurred almost simultaneously for 10s keV to multi-MeV (~5.3 and ~3.4 MeV, respectively), with the inner boundary of the enhancement located at higher L-shell for higher energy
4. The PSD radial gradients of outer-belt relativistic electrons (only reliably estimated for the nonstorm event) are monotonically increasing

All these features combined together provide strong evidence that the identified extremely fast, step-like outer-belt enhancements are most-likely injection-driven. Although we only presented two cases, they imply that even single strong injection events can lead to significant and persistent outer-belt electron enhancements. This observation lends support to earlier studies that suggested that strong MeV electron injections, if occur in a series, may be a crucial contributor to radiation belt enhancement (e.g., Dai et al., 2014; Fok et al., 2001; Glocer et al., 2011; Ingraham et al., 2001; Kim et al., 2000; Nagai et al., 2006; Sorathia et al., 2018).

It remains a topic for future study to determine how often such step-like enhancements occurred and whether they are indeed an important process for radiation belt enhancement. We speculate that during a series of substorm (or flow-burst) dipolarizations, previously injected (and accumulated) electrons are also picked up by penetrating dipolarization electric fields (e.g., Gabrielse et al., 2017) and transported further inward with adiabatic acceleration, which would be similar to the process for impulsive enhancements of ring current ions at encounters of dipolarization front (e.g., Keika et al., 2016). For events of strong multiple dipolarizations, the successive, extremely-fast radial transport may lead to rapid exponential buildup of the outer-belt. Details of this process remains to be examined in future study. Also, future study will need to address how those extremely fast and discrete flux increases can affect accurate estimation of outer-belt PSD radial profiles.

Data Availability Statement

The authors would like to thank G. Reeves for providing us with LANL-GEO electron data and C.-P. Wang for his helpful discussion. The authors greatly appreciate the Van Allen Probes EMFISIS and ECT teams for providing data utilized in this study. Processing and analysis of the MagEIS and REPT data were supported by Energetic Particle, Composition, and Thermal Plasma (RBSP-ECT) investigation funded under NASA's Prime Contract No. NAS5-01072. All RBSP-ECT data are publicly available at the Web site http://www.RBSP-ect.lanl.gov/. The authors also greatly appreciate the SuperMAG collaborators (http://supermag.jhuapl.edu/info/?page=acknowledgement) for providing SuperMAG data. The authors acknowledge the use of

NASA/GSFC's Space Physics Data Facility's OMNIWeb and CDAWeb data. The LANL-GEO data used for this study are available at https://zenodo.org/deposit/4705929.

Acknowledgments
This work was supported by the NASA Grant 80NSSC18K0666. D.-Y. Lee acknowledges support from National Research Foundation of Korea under Grant NRF-2019R1A2C1003140.

References

Agapitov, O., Mourenas, D., Artemyev, A., Hospodarsky, G., & Bonnell, J. W. (2019). Time scales for electron quasi-linear diffusion by lower-band chorus waves: The effects of ωpe/ωce dependence on geomagnetic activity. *Geophysical Research Letters*, *46*, 6178–6187. https://doi.org/10.1029/2019GL083446

Anderson, B. R., Millan, R. M., Reeves, G. D., & Friedel, R. H. W. (2015). Acceleration and loss of relativistic electrons during small geomagnetic storms. *Geophysical Research Letters*, *42*, 10113–10119. https://doi.org/10.1002/2015GL066376

Baker, D. N., Kanekal, S. G., Hoxie, V. C., Batiste, S., Bolton, M., Li, X., et al. (2012). The relativistic electron-proton telescope (REPT) instrument on board the radiation belt storm probes (RBSP) spacecraft: Characterization of earth's radiation belt high-energy particle populations. *Space Science Reviews*, *179*, 337–381. https://doi.org/10.1007/s11214-012-9950-9

Baker, D. N., Li, X., Blake, J. B., & Kanekal, S. (1998). Strong electron acceleration in the Earth's magnetosphere. *Advances in Space Research*, *21*, 609–613. https://doi.org/10.1016/s0273-1177(97)00970-8

Blake, J. B., Carranza, P. A., Claudepierre, S. G., Clemmons, J. H., Crain, W. R., Dotan, Y., et al. (2013). The Magnetic Electron Ion Spectrometer (MagEIS) Instruments aboard the Radiation Belt Storm Probes (RBSP) spacecraft, *Space Science Reviews*, *179*, 383–421. https://doi.org/10.1007/S11214-013-9991-8

Borovsky, J. E., & Yakymenko, K. (2017). Substorm occurrence rates, substorm recurrence times, and solar wind structure. *Journal of Geophysical Research: Space Physics*, *122*, 2973–2998. https://doi.org/10.1002/2016JA023625

Brautigam, D. H., & Albert, J. M. (2000). Radial diffusion analysis of outer radiation belt electrons during the October 9, 1990, magnetic storm. *Journal of Geophysical Research*, *105*, 291–309. https://doi.org/10.1029/1999JA900344

Dai, L., Wang, C., Duan, S., He, Z., Wygant, J. R., Cattell, C. A., et al. (2015). Near-Earth injection of MeV electrons associated with intense dipolarization electric fields: Van Allen Probes observations. *Geophysical Research Letters*, *42*, 6170–6179. https://doi.org/10.1002/2015GL064955

Dai, L., Wygant, J. R., Cattell, C. A., Thaller, S., Kersten, K., Breneman, A., et al. (2014). Evidence for injection of relativistic electrons into the Earth's outer radiation belt via intense substorm electric fields. *Geophysical Research Letters*, *41*, 1133–1141. https://doi.org/10.1002/2014GL059228

Fok, M.-C., Moore, T. E., & Spjeldvik, W. N. (2001). Rapid enhancement of radiation belt electron fluxes due to substorm dipolarization of the geomagnetic field. *Journal of Geophysical Research*, *106*, 3873–3881. https://doi.org/10.1029/2000JA000150

Foster, J. C., Erickson, P. J., Baker, D. N., Claudepierre, S. G., Kletzing, C. A., Kurth, W., et al. (2014). Prompt energization of relativistic and highly relativistic electrons during a substorm interval: Van Allen Probes observations. *Geophysical Research Letters*, *41*, 20–25. https://doi.org/10.1002/2013GL058438

Gabrielse, C., Angelopoulos, V., Harris, C., Artemyev, A., Kepko, L., & Runov, A. (2017). Extensive electron transport and energization via multiple, localized dipolarizing flux bundles. *Journal of Geophysical Research: Space Physics*, *122*, 5059–5076. https://doi.org/10.1002/2017JA023981

Glocer, A., Fok, M.-C., Nagai, T., Tóth, G., Guild, T., & Blake, J. (2011). Rapid rebuilding of the outer radiation belt. *Journal of Geophysical Research*, *116*, A09213. https://doi.org/10.1029/2011JA016516

Horne, R. B., Thorne, R. M., Shprits, Y. Y., Meredith, N. P., Glauert, S. A., Smith, A. J., et al. (2005). Wave acceleration of electrons in the Van Allen radiation belts. *Nature*, *437*, 227–230. https://doi.org/10.1038/nature03939

Ingraham, J. C., Cayton, T. E., Belian, R. D., Christensen, R. A., Friedel, R. H. W., Meier, M. M., et al. (2001). Substorm injection of relativistic electrons to geosynchronous orbit during the great magnetic storm of March 24, 1991. *Journal of Geophysical Research*, *106*, 25759–25776. https://doi.org/10.1029/2000JA000458

Keika, K., Seki, K., Nosé, M., Machida, S., Miyoshi, Y., Lanzerotti, L. J., et al. (2016). Storm time impulsive enhancements of energetic oxygen due to adiabatic acceleration of preexisting warm oxygen in the inner magnetosphere. *Journal of Geophysical Research: Space Physics*, *121*, 7739–7752. https://doi.org/10.1002/2016JA022384

Kellogg, P. J. (1959). Possible explanation of the radiation observed by Van Allen at high altitudes in satellites. *Nuovo Cimento*, *11*, 48–66. https://doi.org/10.1007/BF02724906

Kim, H.-J., Chan, A. A., Wolf, R. A., & Birn, J. (2000). Can substorms produce relativistic outer belt electrons? *Journal of Geophysical Research*, *105*, 7721–7735. https://doi.org/10.1029/1999JA900465

Kim, H.-J., Lyons, L., Pinto, V., Wang, C.-P., & Kim, K.-C. (2015). Revisit of relationship between geosynchronous relativistic electron enhancements and magnetic storms. *Geophysical Research Letters*, *42*, 6155–6161. https://doi.org/10.1002/2015GL065192

Kletzing, C. A., Kurth, W. S., Acuna, M., MacDowall, R. J., Torbert, R. B., Averkamp, T., et al. (2013). The Electric and Magnetic Field Instrument Suite and Integrated Science (EMFISIS) on RBSP. *Space Science Reviews*, *179*, 127–181. https://doi.org/10.1007/s11214-013-9993-6

Kress, B. T., Hudson, M. K., & Paral, J. (2014). Rebuilding of the Earth's outer electron belt during 8-10 October 2012. *Geophysical Research Letters*, *41*, 749–754. https://doi.org/10.1002/2013GL058588

Liu, S., Yan, Q., Yang, C., Zhou, Q., He, Z., He, Y., et al. (2018). Quantifying extremely rapid flux enhancements of radiation belt relativistic electrons associated with radial diffusion. *Geophysical Research Letters*, *45*, 1262–1270. https://doi.org/10.1002/2017GL076513

Mauk, B. H., Fox, N. J., Kanekal, S. G., Kessel, R. L., Sibeck, D. G., & Ukhorskiy, A. (2013). Science objectives and rationale for the radiation belt storm probes mission. *Space Science Reviews*, *179*, 3–27. https://doi.org/10.1007/s11214-012-9908-y

Millan, R. M., & Baker, D. N. (2012). Acceleration of particles to high energies in Earth's radiation belts. *Space Science Reviews*, *173*, 103–131. https://doi.org/10.1007/s11214-012-9941-x

Nagai, T. (2012). Rebuilding process of the outer electron radiation belt: The spacecraft akebono observations. *Geophysical Monograph Series*, *199*, 177–188. https://doi.org/10.1029/2012GM001281

Nagai, T., Yukimatu, A. S., Matsuoka, A., Asai, K. T., Green, J. C., Onsager, T. G., & Singer, H. J. (2006). Timescales of relativistic electron enhancements in the slot region. *Journal of Geophysical Research*, *111*, A11205. https://doi.org/10.1029/2006JA011837

Newell, P. T., & Gjerloev, J. W. (2011). Evaluation of SuperMAG auroral electrojet indices as indicators of substorms and auroral power. *Journal of Geophysical Research*, *116*, A12211. https://doi.org/10.1029/2011JA016779

Olson, W., & Pfitzer, K. (1977). Magnetospheric magnetic field modeling. *Annu. Sci. Rep. AFOSR F44620-75-C-0033*. Huntington Beach, CA: McDonnell Douglas.

Pfitzer, K. A., & Winckler, J. R. (1968). Experimental observation of a large addition to the electron inner radiation belt after a solar flare event. *Journal of Geophysical Research*, *73*, 5792–5797. https://doi.org/10.1029/JA073i017p05792

Pinto, V. A., Kim, H.-J., Lyons, L. R. & Bortnik, J. (2018). Interplanetary parameters leading to relativistic electron enhancement and persistent depletion events at geosynchronous orbit and potential for prediction. *Journal of Geophysical Research: Space Physics*, *123*(2), 1134–1145. https://doi.org/10.1002/2017ja024902

Reeves, G. D., Belian, R. D., & Fritz, T. A. (1991). Numerical tracing of energetic particle drifts in a model magnetosphere. *Journal of Geophysical Research*, *96*, 13997–14008. https://doi.org/10.1029/91JA01161

Reeves, G. D., Friedel, R. H. W., Larsen, B. A., Skoug, R. M., Funsten, H. O., Claudepierre, S. G., et al. (2016). Energy-dependent dynamics of keV to MeV electrons in the inner zone, outer zone, and slot regions. *Journal of Geophysical Research: Space Physics*, *121*, 397–412. https://doi.org/10.1002/2015JA021569

Schiller, Q., Li, X., Blum, L., Tu, W., Turner, D. L., & Blake, J. B. (2014). A nonstorm time enhancement of relativistic electrons in the outer radiation belt. *Geophysical Research Letters*, *41*, 7–12. https://doi.org/10.1002/2013GL058485

Sorathia, K. A., Ukhorskiy, A. Y., Merkin, V. G., Fennell, J. F., & Claudepierre, S. G. (2018). Modeling the depletion and recovery of the outer radiation belt during a geomagnetic storm: Combined MHD and test particle simulations. *Journal of Geophysical Research: Space Physics*, *123*, 5590–5609. https://doi.org/10.1029/2018JA025506

Spence, H. E., Reeves, G. D., Baker, D. N., Blake, J. B., Bolton, M., Bourdarie, S., et al. (2013). Science goals and overview of the radiation belt storm probes (RBSP) energetic particle, composition, and thermal plasma (ECT) suite on NASA's Van Allen Probes mission. *Space Science Reviews*, *179*, 311–336. https://doi.org/10.1007/s11214-013-0007-5

Su, Z., Zhu, H., Xiao, F., Zheng, H., Wang, Y., Zong, Q. G., et al. (2014). Quantifying the relative contributions of substorm injections and chorus waves to the rapid outward extension of electron radiation belt. *Journal of Geophysical Research: Space Physics*, *119*, 10023–10040. https://doi.org/10.1002/2014JA020709

Summers, D., Thorne, R. M., & Xiao, F. (1998). Relativistic theory of wave-particle resonant diffusion with application to electron acceleration in the magnetosphere. *Journal of Geophysical Research*, *103*, 20487–20500. https://doi.org/10.1029/98JA01740

Tang, C. L., Zhang, J.-C., Reeves, G. D., Su, Z. P., Baker, D. N., Spence, H. E., et al. (2016). Prompt enhancement of the Earth's outer radiation belt due to substorm electron injections. *Journal of Geophysical Research: Space Physics*, *121*, 11826–11838. https://doi.org/10.1002/2016JA023550

Thorne, R. M., Li, W., Ni, B., Ma, Q., Bortnik, J., Chen, L., et al. (2013). Rapid local acceleration of relativistic radiation-belt electrons by magnetospheric chorus. *Nature*, *504*, 411–414. https://doi.org/10.1038/nature12889

Tsyganenko, N. A. (1989). A magnetospheric magnetic field model with a warped tail current sheet. *Planetary and Space Science*, *37*, 5–20. https://doi.org/10.1016/0032-0633(89)90066-4

Tsyganenko, N. A., & Sitnov, M. I. (2005). Modeling the dynamics of the inner magnetosphere during strong geomagnetic storms. *Journal of Geophysical Research*, *110*, A03208. https://doi.org/10.1029/2004JA010798

Tverskaya, L. V. (1996). The latitude position dependence of the relativistic electron maximum as a function of Dst. *Advances in Space Research*, *18*(8), 135–138. https://doi.org/10.1016/0273-1177(95)00982-5

Van Allen, J. A., Ludwig, G. H., Ray, E. C., & McIlwain, C. E. (1958). Observation of high intensity radiation by satellites 1958 alpha and gamma. *Journal of Jet Propulsion*, *28*, 588–592. https://doi.org/10.2514/8.7396

Van Allen, J. A., McIlwain, C. E., & Ludwig, G. H. (1959). Radiation observations with satellite 1958 ε. *Journal of Geophysical Research*, *64*, 271–286. https://doi.org/10.1029/JZ064i003p00271